Cell, Vol. 78, 125–136, July 15, 1994, Copyright © 1994 by Cell Press

Rotation of Photoreceptor Clusters in the Developing Drosophila Eye Requires the *nemo* Gene

Kwang-Wook Choi and Seymour Benzer
Division of Biology
California Institute of Technology
Pasadena, California 91125

Summary

The Drosophila eye consists of a reiterative hexagonal array of photoreceptor cell clusters, the ommatidia. During normal morphogenesis, the clusters in the dorsal or ventral halves of the disc rotate 90° in opposite directions, forming mirror images across a dorsoventral equator. In the mutant *nemo* (*nmo*), there is an initial turning of approximately 45°, but further rotation is blocked. Genetic mosaic analysis indicates that the *nmo* gene acts upon each cluster as a whole; normal *nmo* function in one or more photoreceptor cells appears to be sufficient to induce full rotation. The *nmo* gene sequence encodes a serine/threonine protein kinase homolog, suggesting that the kinase is required to initiate the second step of rotation. In another mutant, *roulette*, excessive rotation through varying angles occurs in many ommatidia. This defect is suppressed by *nmo*, indicating that *nmo* acts upstream in a rotation-regulating pathway.

Introduction

Cellular interactions in morphogenesis drive cell shape, rearrangement, and directed movement (Rutishauser and Jessell, 1988; Gumbiner, 1992). Such mechanisms are common, for example, in gastrulation of vertebrate and invertebrate embryos, and evagination of the Drosophila imaginal discs (Fristrom, 1976). One type of movement involves rotation of groups of cells. During somitogenesis in Xenopus, clusters of epithelial cells rotate 90° before differentiating into the segmental muscles and vertebrae, and rotation proceeds in sequence from anterior to posterior (Hamilton, 1969). In Drosophila, the male terminalia rotate 360° during pupal development (Gleichauf, 1936). Two optic ganglia, the lamina and medulla, are initially perpendicular to each other, but fall in line as the medulla rotates 90° during development (White and Kankel, 1978). Rotation is also a common phenomenon in vertebrate embryonic development (Deuchar, 1971).

In the Drosophila eye, the developing photoreceptor clusters in the 800 or so ommatidia rotate 90° during morphogenesis (Ready et al., 1976; Tomlinson and Ready, 1987). This is essential for the formation of a proper ommatidial pattern, and the genes involved can be identified by appropriate mutants. We describe here a gene, *nemo* (*nmo*), that is involved; it is named after the Korean word for a four-sided figure, since the external mutant phenotype is a square, rather than hexagonal, array of facets.

The normal adult eye is built in mirror images across an equator; the trapezoidal pattern of photoreceptor cell clusters in the dorsal half is a reflection of the ventral half (Dietrich, 1909). An early event in eye development during the third larval instar is the sequential clustering of photoreceptor precursors by specific cell–cell interactions (Ready et al., 1976; for recent reviews, see Banerjee and Zipursky, 1990; Greenwald and Rubin, 1992). As this occurs, the clusters in the dorsal and ventral halves rotate by 90° in opposite directions. This rotation vector has two components, direction and degree. First, each cluster must decide to turn either clockwise or counterclockwise, according to whether it is dorsal or ventral. Second, each cluster moves as a unit to maintain the pattern of assembly. Neither of these mechanisms is understood.

Here we show that mutations in the *nmo* gene, while allowing initiation of rotation of about 45° in the correct direction, block the further 45° turn. The contacts between accessory cells are thus altered, resulting in a square pattern. The *nmo* locus encodes a homolog of serine/threonine protein kinases. The results suggest that the rotation occurs in at least two genetically separable steps, the *nmo* protein kinase being required to complete the process. A second mutant, *roulette* (*rlt*), and its interaction with *nmo* are also discussed.

Results

Isolation of the Mutant *nmo*

nmo^{P1} was isolated among P[*lacZ*, w^+] insertion lines that we generated (B. Mozer, K.-W. C., and S. B., unpublished data). Eyes of *nmo* flies are slightly narrowed anterior–posterior, and the facets are square rather than hexagonal (Figure 1). Tangential sections show that the pigment cell lattice is abnormal, especially at corners, which have disarranged bristle and secondary pigment cells. Occasional ommatidia are fused (three to ten per eye). Most ommatidia have normal numbers of photoreceptor cells, although some lack a few. The phenotype is recessive and fully penetrant. Viability is reduced (10% of normal), and the angle between wings is 15°–30° wider than normal.

nmo Fails to Complete Rotation of the Photoreceptor Clusters

The eight photoreceptors in the normal adult ommatidium are arranged in a characteristic trapezoidal pattern, with R1, R2, and R3 anterior and parallel to the dorsoventral axis. R7 projects into the middle of the cluster, also parallel to the dorsoventral axis, but pointed dorsally in the upper half of the eye, ventrally in the lower half (Figures 2A–2C). In *nmo*, most R cell clusters, although showing the normal trapezoidal pattern, have abnormal orientation. Their angles are confined to a narrow window (Figures 2D–2F). The dorsal and ventral arrays in *nmo*, while still mirror images, face perpendicularly to each other, instead of being antiparallel. The angles of rotation in wild type and *nmo* average 89° ± 6° and 49° ± 17°, respectively, suggesting that rotation in *nmo* is typically blocked half way. This is not fully expressed in all ommatidia; a minority

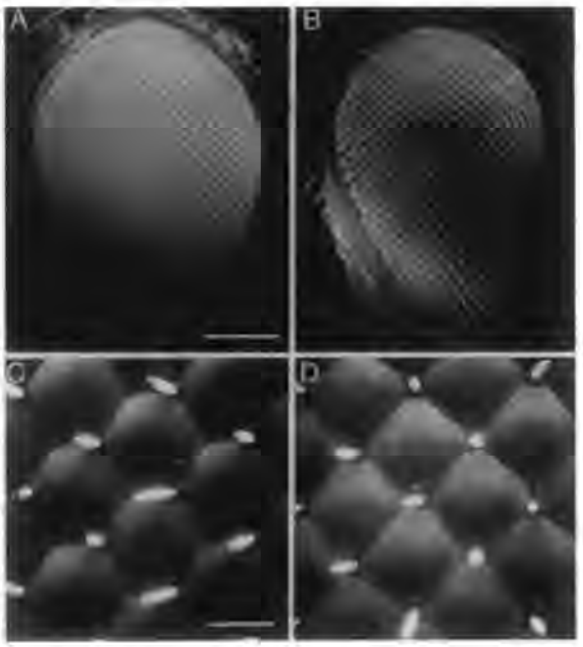

Figure 1. Adult Eye Phenotype of the *nmo* Mutant

Scanning electron microscopy of the wild-type eye (A and C) shows a hexagonal array of ommatidia. The *nmo* eye (B and D) has an essentially square array and is narrower along the anterior–posterior axis. Anterior is to the right. Scale bars in (A) and (B), 100 μm; in (C) and (D), 10 μm.

of approximately 13% (307 of 2376 ommatidia scored from 17 eyes) have essentially normal angles.

We examined the orientations of developing photoreceptor clusters in eye discs, using anti-elav antibody, which cross-reacts with neurons (Robinow and White, 1991). An early event in eye morphogenesis is the establishment of 5-cell preclusters of cells R8, R2, R5, R3, and R4. These are arranged symmetrically about a midline that bisects R8 and divides R2/R3 on one side from R4/R5 on the other (see ommatidium in round brackets in Figures 3A–3B) (Tomlinson and Ready, 1987). They become complete 8-cell clusters as they are joined by cells R1 and R6, then R7 (see ommatidium in square brackets in Figures 3A–3B). As the clusters mature, the nuclei of R8 cells sink basally, while R7 cell nuclei rise apically to the former R8 positions (Tomlinson, 1985). As an indicator of ommatidial orientation in preclusters, we used a line that passes between R3 and R4 and bisects R8; in the 8-cell clusters, we used R7 (Figures 3C–3D). In wild type, the 5-cell preclusters are, early on, rotated approximately 45° (columns 1–4 posterior to the advancing furrow in Figure 3). In columns 5–7, some have completed a 90° rotation, as have most of those posterior to column 7 (Figures 3A and 3C). In *nmo* eye discs, on the other hand, a great majority of the ommatidia show the initial rotation, but do not continue to 90° (Figures 3B and 3D).

During pupal development, four cone cells are added apically to the photoreceptor cluster, followed by two primary pigment cells, which surround the anterior and posterior cone cells. The addition of new pattern elements is highly stereotypic, involving precise cell–cell contacts (Cagan and Ready, 1989). We compared the cone cell patterns of wild type and *nmo* in the pupal stage, to see whether they are abnormally rotated in *nmo*, by using cobalt sulfide staining to visualize the apical surface of the retina (Melamed and Trujillo-Cenóz, 1975). By 45 hr after puparium formation, the wild-type eye showed a hexagonal lattice, with bristles and secondary and tertiary pigment cells in their final positions, and the cone cells consisting of an anterior–posterior pair and a dorsoventral pair (Figure 3E). *nmo* pupal eyes also showed a proper set of four cone cells (except that, occasionally, there were five). However, like the R cell clusters, the cone cells and primary pigment cells were rotated about 45° from normal (Figure 3F). This suggests that the abnormal angles in the pupal and, eventually, the adult eye follow the preexisting pattern set by the photoreceptor clusters in the disc.

Apparently, the consequences of the abnormal contacts are mispositioning of bristles, lack of tertiary pigment cells, and lack of the expanded horizontal secondary pigment cells that normally connect a bristle and a tertiary pigment cell, thus leading to the square array of the *nmo* eye.

nmo Acts within the Ommatidium

The rotation of photoreceptor clusters could be regulated by a signal arising within each ommatidium, or by interaction with neighbors via diffusible factors. To distinguish between these possibilities, mosaic eyes were generated by X-ray-induced mitotic recombination. We used $nmo^{147\text{-}1}$, a w^- imprecise excision allele (see Experimental Procedures), and P[w^+]33, a strain with a closely linked P[w^+] insertion at 70C (Carthew and Rubin, 1990), to generate w^- mutant patches surrounded by $nmo^{147\text{-}1}$/P[w^+]33 normal ommatidia. Of ommatidia examined at the mosaic boundary, where mixtures of genotypically normal and mutant cells were present, a majority were normal, but a significant number of ommatidia (14%, 38 of 267) still showed abnormal rotation. Similar results were obtained from mosaic eyes generated using nmo^{P1} (data not shown). These suggest local autonomy of the determination of rotation, i.e., not a long-range influence extending into an all-mutant area from the area of normal cells (Figure 4; Tables 1 and 2). The photoreceptors within mutant ommatidia showed an essentially normal trapezoidal pattern, each photoreceptor cluster apparently rotating as a unit.

To determine whether a specific subset of photoreceptor cells requires nmo^+ function for normal rotation, the genotypes of individual photoreceptor cells were scored at mosaic boundaries, choosing only ommatidia involving a mixture of w^+ and w^- pigment cells, photoreceptor cells, or both. The results are given in Figure 4 and Table 1. When one or more of the photoreceptor cells in an ommatidium was nmo^+, rotation was normal 95% of the time (197 of 207); there was a rapid rise in normal rotation when the number of normal photoreceptors increased from zero to one. No evidence was found that nmo^+ function was required in any particular photoreceptor cell; nmo^+ in any of them was sufficient. Note, however, that, in the boundary

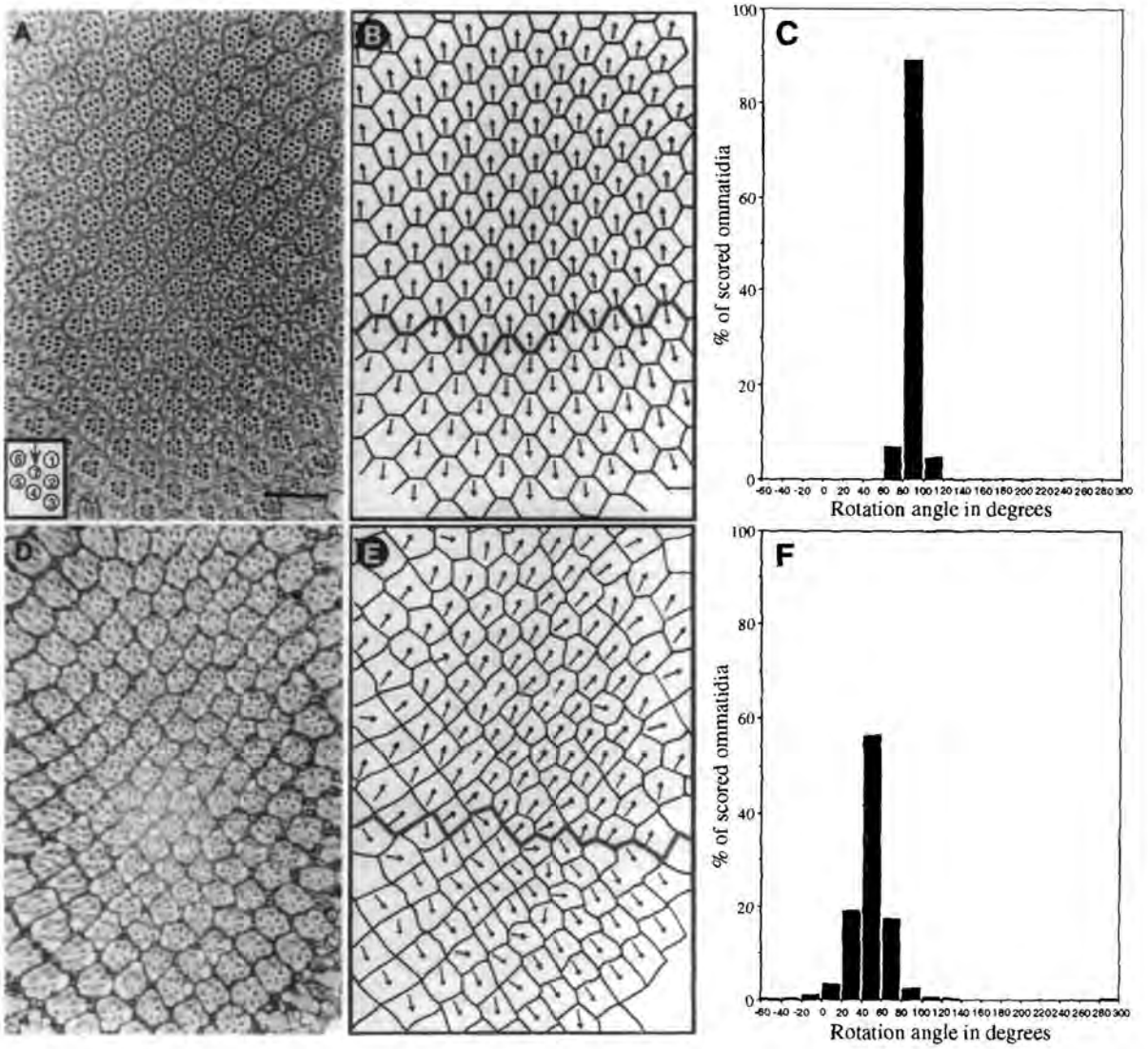

Figure 2. Abnormal Orientation of Photoreceptor Clusters in the *nmo* Eye

(A and D) Tangential section through wild-type adult and *nmo* eyes. The wild type (A) shows the normal lattice; R1, R2, and R3 cells face anteriorly; R5 and R6 are posterior, and R7 projects vertically, between R1 and R6, and parallel to R1, R2, and R3 (see inset at the lower left corner). The dorsal and ventral halves of the eye are mirror images across the equator (thick line in [B] and [E]). In *nmo* (D), while dorsal and ventral ommatidia are still mirror images, the photoreceptor clusters are typically rotated by about 45° from normal.

(B and E) Schematic drawings of (A) and (D), respectively; arrows indicate the projected directions of R7 as markers for ommatidial orientation. In the normal eye, dorsal and ventral R7 cells are perpendicular to the equator and antiparallel. In *nmo*, they are perpendicular to each other, owing to the incomplete rotation. Scale bar, 50 μm.

(C and F) Histograms for angles of rotation in the wild type (C) and *nmo* (F), measured for each photoreceptor cluster with respect to a best-fit equatorial line. In one eye each of three wild-type flies, 505 ommatidia were scored, and in one eye each of seven *nmo* flies, 943 ommatidia were scored. The wild type and *nmo* show peaks at 80°–100° and 40°–60° intervals, respectively.

ommatidia, 53% of those lacking nmo^+ photoreceptor cells nevertheless rotated normally, a level significantly higher than the background rate of 18% (39 of 206) observed in all-*white* areas of the mosaics, or the 13% seen earlier for the nmo^{P1} allele. The question of whether this effect could be related to the secondary pigment cells is addressed in Table 2, which further analyzes the subgroup of boundary ommatidia that contained no nmo^+ photoreceptors. The proportion of normal rotations within that group was indifferent to the number of nmo^+ secondary pigment cells surrounding an ommatidium. Our interpretation of these data is that each ommatidium rotates as an essentially autonomous unit, triggered by the presence of one or more photoreceptor cells of nmo^+ genotype, and that there may be some leakage of the signal that can, over a very short range, influence neighboring photoreceptor clusters.

The *nmo* Mutation Suppresses the Rotation Defect of the Mutant *rlt*

The *rlt* mutant was isolated because of its roughened eye surface and was found to be strikingly abnormal in photo-

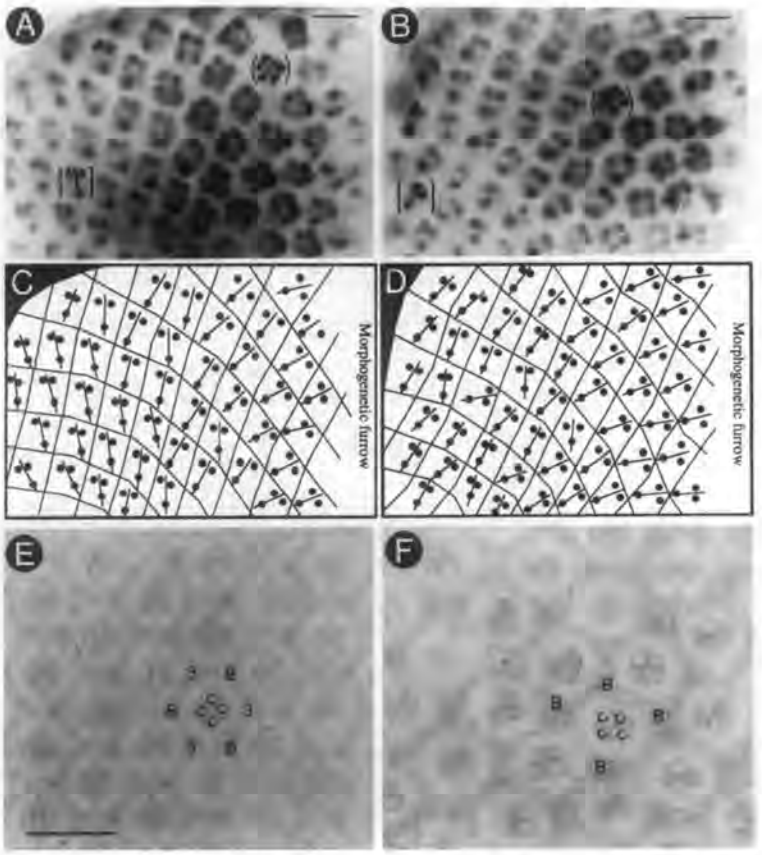

Figure 3. Incomplete Rotation of Photoreceptor Clusters in the Developing Eye

Third instar eye discs were stained with anti-elav antibody to visualize photoreceptor cells. Cluster formation proceeds in a wave behind the morphogenetic furrow, which advances from posterior to anterior (left to right in the figure). (A), wild type; (B), *nmo*. Round brackets show the photoreceptor cell nuclei of preclusters close behind the morphogenetic furrow. More mature 8-cell clusters are posterior to the 5-cell preclusters. One of these in each disc is indicated by square brackets; only R3, R4, and R7 cells are clearly seen at this focal plane. Arrows indicate orientation by the midline that passes between R3 and R4 and bisects R7 or R8. In (C) and (D), R3/R4/R8 (for 5-cell preclusters) or R3/R4/R7 (for 8-cell clusters) highlight the orientations of each cluster. In the wild-type disc, the midlines of most 5-cell clusters, close behind the furrow, are already rotated about 45° from the anterior–posterior axis, changing progressively to 90°. In *nmo*, further rotation after the initial step does not occur, although there are occasional exceptions. The fields of view in both cases are above the equator. Note that, at this stage of development, both wild-type and *nmo* arrays are square. (E–F) Pupal eyes stained with cobalt sulfide to accentuate cell membranes at the apical level. (E) Wild type. By 45 hr after puparium formation, four cone cells have arisen apically, enwrapping the apical tips of the photoreceptors (which are not seen at this level). The group of four cone cells is surrounded by two primary pigment cells, one anterior, the other posterior (see Cagan and Ready, 1989, for details of pupal eye development). The hexagonal shape of the ommatidium is already evident. (F) *nmo* pupal retina of the same age; it fails to form the hexagonal pattern. The cone cell clusters and the primary pigment cells are all rotated about 45°. P, primary pigment cell; B, bristle; C, cone cell; 3, tertiary pigment cell. Anterior is to the right. Scale bar, 10 μm.

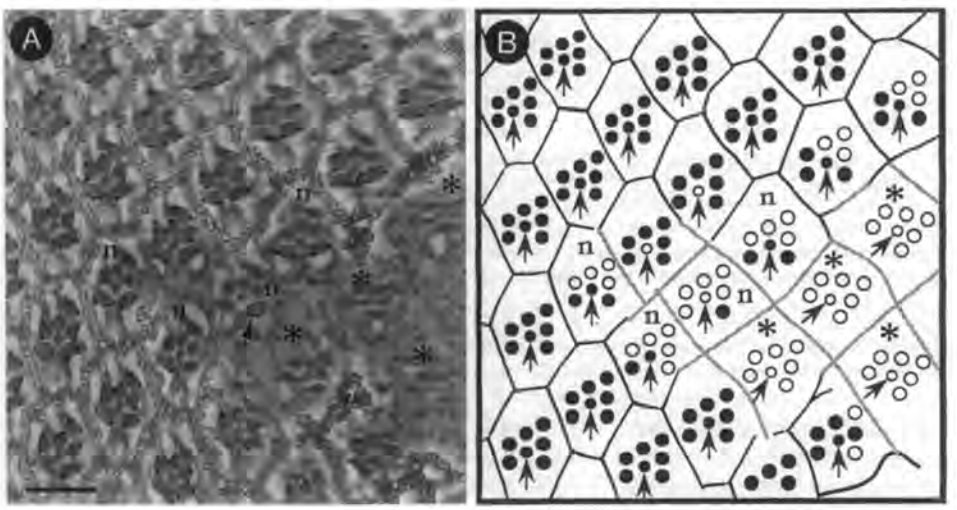

Figure 4. Mosaic Analysis with *nmo*

(A) Section of a mosaic eye showing a white patch of ommatidia surrounded by w^+ pigment cells. Pigment granules in the photoreceptor cells can be seen as dark spots just underneath the rhabdomeres (arrow). Ommatidia surrounded completely by w^+ pigment cells contain nmo^+ photoreceptor cells and show normal orientation. When all photoreceptors are nmo^-, as shown in the ommatidia marked with an asterisk, they show *nmo*-like abnormal orientations. Note that mosaic ommatidia in which only one to three photoreceptors are nmo^+ (marked with the letter n) show normal orientation.

(B) Schematic drawing of the mosaic eye section. The solid and dotted lines between ommatidia indicate secondary pigment cells of genotypes w^+ nmo^+ and w^- nmo^-, respectively. Wild-type and w^- nmo^- photoreceptors are represented by closed and open circles, respectively. The arrows indicate the orientation of R7. Anterior is to the right. Scale bar, 10 μm.

Table 1. Results of Mosaic Analysis: Effect of Photoreceptor Cell Genotype

Number of w^+ nmo^+ R Cells	Normal Rotation	Abnormal Rotation	Percent Normal
0	32	28	53
1	27	3	90
2	11	4	73
3	20	1	95
4	15	1	94
5	11	0	100
6	21	0	100
7	23	0	100
8	69	1	99
Ommatidia with one or more w^+ R cell	197	10	95

Effect on rotation of the genotypes of photoreceptor cells within an ommatidium. Ommatidia scored were all at boundaries of mosaic patches, defined by the requirement that the secondary pigment cells surrounding an ommatidium, the inside photoreceptor cells, or both were of mixed mutant and normal genotypes, using w^+ as a marker linked to *nmo*. Ommatidia containing one or more w^+ nmo^+ photoreceptor cells have a high probability of normal rotation.

receptor orientation (Leiserson and Benzer, unpublished data). The majority of ommatidia have a normal number of photoreceptor cells, in proper trapezoidal configuration, except that some have an additional photoreceptor cell (17% of 545 ommatidia scored in one eye each of four flies). Although an equator is evident, the rotation angles show a very broad distribution (Figures 5A–5C). Of the photoreceptor clusters in *rlt*, 47% (615 ommatidia scored in one eye each of six flies) actually rotate more than 90° which is rare in wild type and *nmo* (Figure 5B). This suggests that *rlt* is unable to arrest rotation beyond the normal 90°. Eyes of the *nmo rlt* double mutant were examined for phenotypic interaction between the two mutations. Surprisingly, the majority of ommatidia in *nmo rlt* have a similar phenotype to *nmo*. The number of ommatidia with rotation over 100° is decreased to 9% (based on 807 ommatidia scored in one eye each of nine flies), and the main distribution of angles is returned to around 45°, as in *nmo* (Figures 5D–5F). This suggests that *nmo* is epistatic to *rlt*, the *nmo* gene acting upstream in the same pathway. It is also interesting to note that, in *nmo rlt*, the number of ommatidia with an additional photoreceptor cell decreased more than 3-fold (5% of 730 ommatidia scored in one eye each of six flies). Although the ommatidial orientations in the double-mutant eyes are more or less like *nmo*, the rotation angles have a slightly wider range. It is unclear whether that is owing to incomplete suppression of the *rlt* defect by *nmo*, or to other defects of the *rlt* mutation.

Isolation of the *nmo* Gene

The P[*lacZ*, w^+] insertion was localized by in situ hybridization to region 66B1-2 on the left arm of the third chromosome. The P element was mobilized by dysgenic crosses to generate revertants (see Experimental Procedures). Of the w^- revertants (73 of a total 153 lines tested), 48% showed normal eyes, demonstrating that the eye phenotype was indeed caused by the insertion. Another gene, *pebble* (*pbl*), maps to the same region 66B1 (Hime and Saint, 1992), and chromosomes deficient in *pbl* were used to map *nmo*. In heterozygotes, the large deficiencies *Df(3L)pbl*^{X1} and *Df(3L)pbl*^{NR}, which lack, respectively, regions 65F3-66B9 and 66B1-2, uncovered the *nmo* gene, but *Df(3L)8* and *Df(3L)25* complemented the *nmo* eye phenotype. Therefore, the *nmo* gene is between the proximal breakpoints of the deficiencies *Df(3L)25* and *Df(3L)pbl*^{NR}, and *pbl* is distal to *nmo* (Figure 6A).

Genomic DNA flanking the P element was isolated by plasmid rescue (Pirrotta, 1986) and used to isolate cosmid clones of the region. Inserts from cosmids cos3a and cos2b, which overlap by 10 kb, including the transposon insertion site, were used to screen adult head cDNA libraries, and clones positive for both were characterized (Figure 6B). The cDNAs were classified into two differentially spliced forms, type I and type II, alike in the 5′ region but different in the 3′ (Figure 6B; see also Figure 8). The direction of *nmo* transcription is opposite to that of the *lacZ* transcription of the original P[*lacZ*, w^+] insert, as deter-

Table 2. Results of Mosaic Analysis: Effect of Pigment Cell Genotype

Number of w^+ nmo^+ Pigment Cells	Normal Rotation	Abnormal Rotation
1	14	16
2	7	8
3	6	3
4	1	1
5	4	0
Ommatidia with one or more w^+ pigment cell	32	28

Further analysis of the 60 boundary ommatidia that contained no w^+ photoreceptor cells (top line of Table 1). The number of surrounding secondary pigment cells apparently has no effect on the probability of normal rotation.

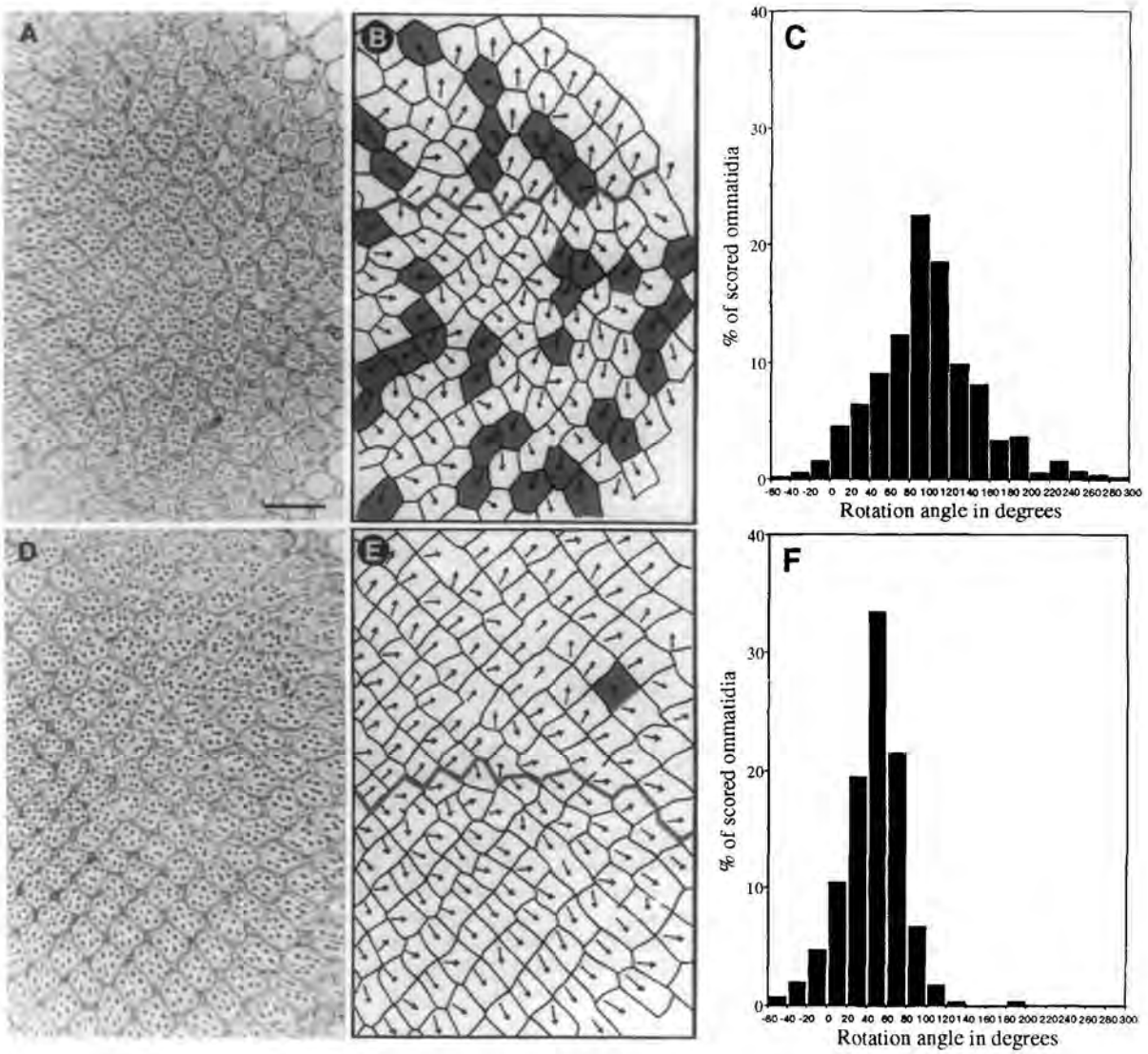

Figure 5. Suppression of the *rlt* Rotation Defect by *nmo*

(A) Section of a *rlt* eye. The orientations of photoreceptor clusters are widely variable.

(D) *nmo rlt* double mutant. The orientations of most photoreceptor clusters are returned to around 45°, as in the *nmo* eye.

(B and E) Schematic drawings of (A) and (B), respectively. Arrows indicate the directions of R7 as markers for ommatidial orientation. Ommatidia rotated more than 110° are shaded. Notice the great decrease in the number of shaded ommatidia in *nmo rlt*.

(C and F) Histograms showing the distributions of rotation in *rlt* and *nmo rlt*. In one eye each of six *rlt* flies, 615 ommatidia were scored, and in one eye each of nine *nmo rlt* flies, 807 ommatidia were scored. The negative angle values (−1° to −60°) represent either reverse rotation or rotation of 300°–359° in the correct direction, which cannot be distinguished. The pattern of angular distribution in *nmo rlt* is similar to that of *nmo*, as shown in Figure 2F. Scale bar, 50 μm.

mined by the open reading frame of the cDNA (see Figure 8) and by single-strand mRNA hybridization (see Figure 7).

A Southern blot of cleaved cosmid DNAs probed with type I cDNA C4-2 indicated that the 5′ portion of the cDNA maps within the 2.2 kb EcoRI fragment in which the transposon is inserted, but the 3′ portion is not covered by cos3a (Figure 6B). Additional cosmid clones were isolated using a 3′ region of cDNA C4-2 as probe. The 3′ portion of the cDNA maps within a 5 kb BglII fragment of cosR2-4. The intronic gap between the 5′ and 3′ portions of the cDNA was filled by additional phage and cosmid clones, λMF9 and cos33c (data not shown), which extend over 80 kb. The site of transposon insertion determined by sequencing the rescued plasmid DNA is 1223 bp from the 5′ end of type I cDNA C4-2. One of the type II cDNAs, C5-1, has an additional 153 bp extending beyond the 5′ end of C4-2. Within these 153 bp, 52 bp at the 3′ end are located at 521 bp from the insertion site. The location of the remaining 101 bp has not been identified; it is not covered by cos2b-2, which extends about 30 kb further upstream from the insertion site, suggesting that the entire transcription unit is over 100 kb long. An imprecise excision allele has a deletion of several kilobases downstream but not upstream of the insertion site (Figure 6B), suggesting that

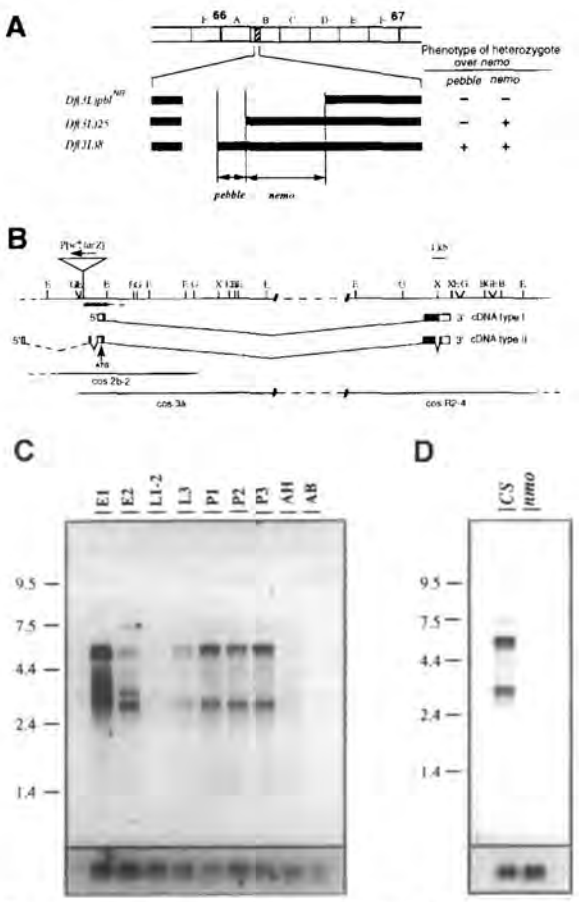

Figure 6. Genetic and Physical Maps of the *nmo* Region

(A) Chromosomes deficient in the *pbl* gene were used to map *nmo*. The large deficiencies *Df(3L)pbl*^{X1} (65F3-66B9, not shown) and *Df(3L)pbl*^{NR} (66B1-2) uncovered *nmo*, but *Df(3L)8* and *Df(3L)25* complemented the *nmo* eye phenotype. Therefore, the *nmo* locus is within the region between the proximal and distal breakpoints of *Df(3L)pbl*^{NR} and *Df(3L)25*, respectively, whereas the *pbl* gene is distal to *nmo*. Blank spaces within the black bar indicate the extent of deletion.

(B) Physical map of the *nmo* gene. The P[*lacZ*, *w*$^+$] element is inserted 1223 bp upstream of the 5′ end of the cDNA C4-2 (type I) and between two 5′ untranslated exons of cDNA C5-1 (type II). The 101 bp 5′ end sequence was not covered by cos2b-2, suggesting that it is more than 30 kb upstream of the P insertion site. The insertion site was determined by sequencing a rescued plasmid, using an oligonucleotide sequence derived from the P element as the sequencing primer. The 5′ portion of the C4-2 cDNA is contained within a 2.2 kb EcoRI genomic fragment near the insertion site. The exon–intron boundaries of the 5′ region of cDNA were determined by sequencing the cDNAs and the 2.2 kb EcoRI genomic fragment. The remaining 3′ region of the cDNA is interrupted by an intron of about 80 kb, and localized within a 5.7 kb BglII fragment of cosmid R2-4. The exon–intron structure of the 3′ region has not been determined. The orientation of *nmo* transcription is opposite to that of *lacZ*. Open and closed squares indicate untranslated and coding sequences respectively. The hatched bar at the insertion site is deleted in *nmo*$^{83\text{-}1}$, an imprecise excision allele. The upstream region of the insertion site is intact. The dotted line indicates uncertainty of the breakpoint. The restriction site: B, BamHI; E, EcoRI; B, BglII; and X, XbaI.

(C) Developmental expression of *nmo* transcripts in wild type. Poly(A)$^+$ RNA was isolated at different stages. In each lane, 2 μg was loaded and probed with random primer–labeled C4-2 cDNA insert. The bands at the bottoms of blots C and D indicate similar amounts of RNA loaded in each lane, as shown by hybridization with a probe from the *rp49* gene that is expressed throughout development (O'Connell and Rosbash, 1984). E1, 0- to 12-hour-old embryo; E2, 12- to 24-hour-old embryo; L1–2, first plus second instar larvae; L3, third instar larva; P1, 0- to 2-day-old pupa; P2, 2- to 4-day-old pupa; P3, 4- to 6-day-old day pupa; AH, adult heads; AB, adult bodies.

(D) *nmo* compared with wild type. Poly(A)$^+$ RNA (2 μg) from pupae of mixed ages was loaded in each lane. All the multiple wild-type transcripts were absent in *nmo*.

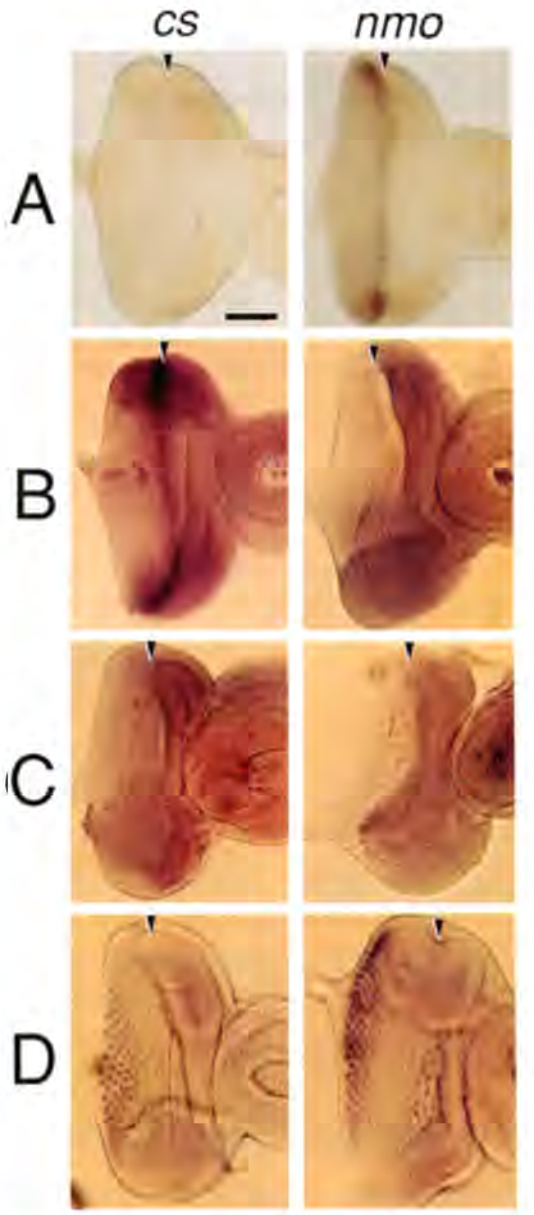

Figure 7. Expression of *nmo* Transcripts in the Eye Disc

(A) LacZ expression detected by anti-β-gal staining. No expression is detected in the Canton-S wild type. The *nmo*^{P1} eye disc shows LacZ expression near the morphogenetic furrow (arrowheads) and at lower levels in other regions posterior to the furrow. (B) Anti-sense C4-2 cDNA probe. This hybridized to the region near the morphogenetic furrow in the wild-type but not in the *nmo* disc. (C) Sense strand C4-2 cDNA probe. No *nmo* expression was detected in either wild type or mutant. (D) Expression of the *chaoptin* transcript was similar in wild type and *nmo*. Scale bar, 50 μm. Anterior is to the right.

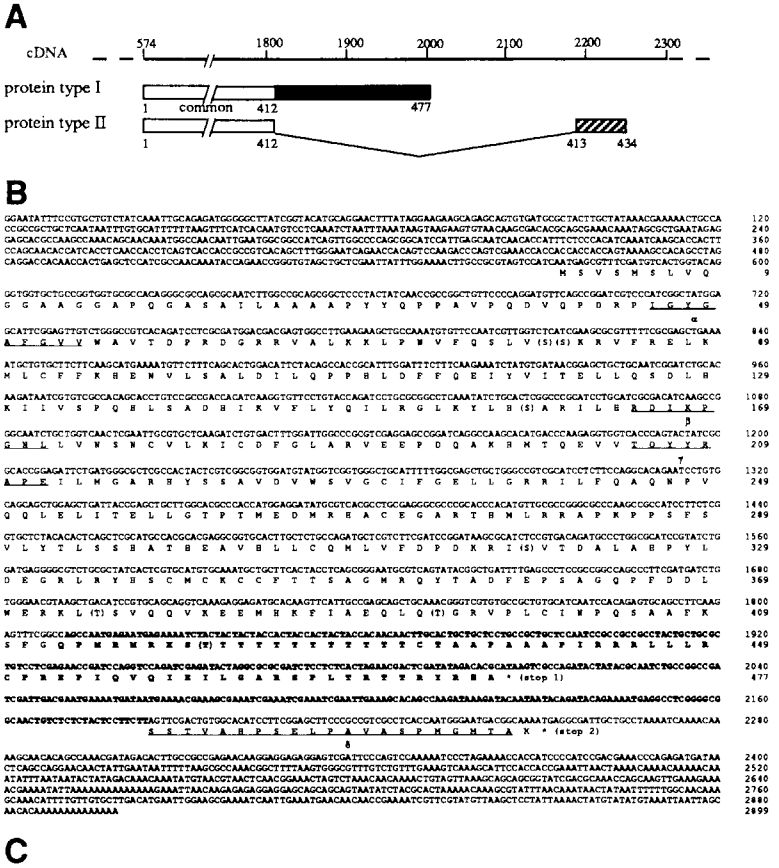

Figure 8. Sequences of Type I and Type II *nmo* cDNAs

(A) Differential splicing produces two types of cDNAs, which are conceptually translated into different polypeptides. Type II cDNA lacks 375 bp near the 3′ end (boldface segment 1810–2184 in [B]).

(B) Composite sequence. Two protein kinase signature sequences that are involved in ATP binding (Hanks et al., 1988) and in catalysis (Knighton et al., 1991) are marked by underlines α and β, respectively. Amino acid residues underlined γ match the consensus sequence for the serine/threonine protein kinase family (Hanks et al., 1988). Potential phosphorylation sites are parenthesized. Because of the deletion in type II, a segment of 65 amino acids (dark box in [A] and boldface in [B]) is missing, containing a stretch of 12 threonines that are potential sites for cAMP-dependent phosphorylation. The reading frames of type I and II cDNAs stop at different sites (stop 1 and stop 2), generating an additional 22 amino acids for type II (hatched box in [A] and underline δ in [B]).

(C) Sequence comparison with other protein kinases. The predicted amino acid sequence of *nmo* is aligned with sequences of two closely related protein kinases, alfalfa MsERK1 kinase (Duerr et al., 1993; 41% identity), rat ERK1 (Boulton et al., 1991; 39% identity), and yeast CDC28 (Lorincz and Reed, 1984; 37% identity). The *nmo* kinase shows the 11 subdomain structures (Roman numerals) characteristic of most known protein kinase genes (Hanks et al., 1988). Threonine and tyrosine residues marked with an asterisk are conserved in the ERK kinase family. The tyrosine residue is replaced by glutamine in Nmo and CDC28 kinases. Shaded letters indicate identical residues.

the first intron is unlikely to be involved. The evidence that the cDNAs we have identified are from the *nmo* gene is as follows: the P[*lacZ, w*$^+$] insertion site is spanned by the cDNAs; remobilization of the transposon reverts the mutant phenotype; the tissue expression patterns of *lacZ* reporter and cDNA hybridization are similar (see below); and transcripts corresponding to the cDNAs are lacking in the mutant (see below).

nmo^{P1} is a Null Allele

Several deletion alleles were generated by remobilizing the P element. None of these, over the *nmo*^{P1} chromo-

some, showed a more severe eye phenotype than that of homozygous nmo^{P1}. Flies heterozygous for two deletion chromosomes, deficient in the 5′ region of the gene, including the N-terminal 55 amino acids, also showed the same phenotype. Furthermore, deletion of the entire gene by deficiencies *Df(3L)pbl*^{NR} and *Df(3L)pbl*^{X1}, which lack 66B1-2 and 65F3-66B9, respectively (Hime and Saint, 1992), did not cause a more severe eye defect. These results suggest that nmo^{P1} is null or a severe hypomorph. All of the multiple transcripts expressed in the wild-type pupa were absent or undetectable in the mutant (Figure 6D).

Expression of the *nmo* Transcripts

Transcripts from the *nmo* locus are expressed throughout development in a complex pattern. Northern hybridization with cDNA C4-2 as a probe detected, in 0- to 12-hour-old embryos, six transcripts (of 3.2, 3.6, 4.1, 4.6, 5.4, and 5.8 kb). In 12- to 24-hour-old embryos, these were reduced, especially the 4.1 and 5.4 kb (Figure 6C). A new, larger transcript of 7.2 kb appeared in the late embryo. Expression of all transcripts was weakest in first and second instar larvae. In third instar larvae, the expression of 3.2, 5.4, and 5.8 kb transcripts increased. This high level was maintained throughout pupal development, but decreased in the adult. The 3.6, 4.1, and 4.6 kb transcripts, abundant in embryos, were not detected in the pupal stages, suggesting that the gene may have early functions in addition to eye development. Adult heads expressed 5.4, 5.8, 7.2, and 7.6 kb transcripts at low levels, but little expression, if any, was seen in adult bodies. The cDNAs from adult head libraries were smaller than 2.7 kb; the overlaps in hand cover about 3 kb. Full-length clones for the various transcripts are yet to be isolated.

Spatial Expression of *nmo*

To localize *nmo* expression, eye discs from third instar larvae were hybridized in situ to *nmo* cDNA probes. A *chaoptin* probe served as a positive control. *nmo* discs showed normal expression of transcripts of *chaoptin*, which encodes an antigen recognized by MAb 24B10 (Zipursky et al., 1984; Reinke et al., 1988) (Figure 7D). Single-stranded anti-sense *nmo* cDNA hybridized to normal discs near the furrow, but, consistent with the Northern blot results, no obvious transcript was detected in *nmo* (Figure 7B). A sense strand DNA probe was negative in both wild type and *nmo* (Figure 7C). We also examined expression of the *lacZ* reporter gene in the nmo^{P1} enhancer trap line by anti-β-gal monoclonal antibody. In the third instar disc, LacZ was expressed strongly near the furrow (Figure 7A), similar to the *nmo* transcript. In addition, weaker staining was also detected in photoreceptor cell precursors posterior to the furrow (data not shown). This may be due to the higher sensitivity of immunocytochemical detection of LacZ.

The *nmo* Gene Encodes a Serine/Threonine Protein Kinase Homolog

The 2899 bp composite sequence of the cDNA clones was determined. Type I and type II cDNAs have open reading frames that can encode polypeptides of 477 and 434 amino acids, respectively, by differential splicing near the 3′ end (Figure 8A). The predicted polypeptide of type II cDNA lacks a segment of 65 amino acids (413–477), but has an additional 22 amino acids (413–434) (Figure 8B). Although the same nucleotide sequence is present in type I, it is there untranslatable, being out of frame with its long open reading frame.

Protein databanks were searched by the FASTA program (Pearson and Lipman, 1988). The predicted protein has extensive similarity to a family of serine/threonine protein kinases. Many of these contain 11 designated subdomains (Hanks et al., 1988); all of these are present in the predicted *nmo* protein (Figure 8C). Also present are two protein kinase signature sequences: the nucleotide-binding site (LIV)GXGX(FY)(SG)X(LIV) in subdomain I, and a sequence RDIKPGN in subdomain VI that is important for catalysis (Knighton et al., 1991). A protein containing the two signature sequences is almost certain to be a protein kinase (Bairoch and Claverie, 1988; Hanks et al., 1988). The type I polypeptide has a stretch of 12 threonine residues following arginine and lysine near the C-terminus (Figure 8B). The sequence (RK)2X(ST) is a potential phosphorylation site for cAMP-dependent protein kinase.

The protein kinase domain of *nmo* is most similar to a family of mitogen-activated protein (MAP) kinases, including plant Ms extracellular signal–regulated protein kinase 1 (ERK1) (Duerr et al., 1993), murine ERK1 (Boulton et al., 1991), and yeast CDC28/cdc2-related genes (Lorincz and Reed, 1984), with 37%–41% identity over a region of about 300 amino acids. However, the similarity of the *nmo*-encoded protein to MAP kinases is limited to the catalytic domain (regions I through XI in Figure 8), so Nmo may not be functionally related to the MAP kinase family. A Drosophila homolog of ERK1 is 80% identical to mammalian ERK1 (Biggs and Zipursky, 1992). Nmo shows a difference from the ERK type. ERK protein kinases have two conserved residues, threonine and tyrosine, in subdomain VIII, a common autophosphorylation region (Hanks et al., 1988); phosphorylation of both threonine (amino acid residue 200, Figure 8) and tyrosine (residue 202) is critical for their function (Payne et al., 1991; Gartner et al., 1992). Nmo has the necessary threonine, but lacks the critical tyrosine. CDC28/cdc2, another non-ERK kinase, also contains the threonine but not the tyrosine (Figure 8C).

Discussion

The dorsoventral symmetry of the eye has long been known (Dietrich, 1909), as well as its generation by rotation during development (Ready et al., 1976; Tomlinson and Ready, 1987; Ready, 1989), but little is understood about the underlying mechanisms. Several mutants, including *disordered facets* (*dif*), *irregular eye* (*ire*), *rugged* (*rug*), and *pomegranate* (*pom*), also show abnormal orientations of ommatidia (Baker et al., 1992). However, these mutations appear to affect cell differentiation, resulting in improper packing of the ommatidia during late pupal development, rather than the primary rotation itself, which occurs in the third instar eye disc.

In *nmo*, the photoreceptor clusters initiate but do not

complete the full rotation. One possibility is that the *nmo*$^+$ gene product provides a necessary mechanical force. If so, running out of steam in the mutant might be expected to cause rotation angles widely distributed between 0° and 90°. However, the angles in *nmo* are in a narrow window (Figure 2). Although that does not exclude the latter model, a more attractive hypothesis is that the rotation occurs in two discrete steps. The two halves of the rotation would be regulated by separate mechanisms, *nmo* being normal in the first step, but its action failing to proceed, owing to a block, in the second.

An important question is whether the rotation of a photoreceptor cluster is autonomous or occurs through neighbor interaction. Rotation occurs normally in the *Ellipse* mutant eye, where the photoreceptor clusters are widely separated, suggesting that it is likely to be autonomous (Baker and Rubin, 1992). Consistent with this, our mosaic analysis shows that, at mosaic boundaries, many ommatidia that lack *nmo*$^+$ photoreceptors fail to be rescued by adjacent normal cells. Our mosaic analysis further suggests that *nmo*$^+$ function in any of the photoreceptor cells, rather than in a specific subset, can be sufficient. It was found, however, that ommatidia at the boundary lacking *nmo*$^+$ photoreceptors have significantly higher probability of normal rotation (53%) than those well inside the mutant patch (18%). One explanation could be that other *nmo*$^+$ cell types are responsible for their normal rotation. If that were so, the probability of normal rotation should not be affected by the presence of *nmo*$^+$ photoreceptor cells. However, the presence of one or more *nmo*$^+$ photoreceptor cells increased the probability of complete rotation from 53% to almost 100% (Table 1). It therefore appears likely that, although the rotation of a photoreceptor cluster occurs by a mechanism essentially intrinsic to an ommatidium, with any *nmo*$^+$ photoreceptor cell in the cluster being sufficient to trigger rotation of the entire group, this signal may occasionally also leak to adjacent groups at a mosaic boundary.

Since the dorsal and ventral halves of the eye are mirror images, there must be a mechanism that directs a cluster to rotate either clockwise or counterclockwise. Our observations show that an equator is present in the *nmo* eye; the rotations, albeit only 45°, are in correct directions above and below. Hence, the mutation does not affect the direction of rotation.

The Drosophila male terminalia normally rotate 360° during the pupal stage (Gleichauf, 1936); mutations in the *head involution defective* (*hid*) gene cause rotational abnormalities in them, in addition to other developmental defects (Abbott and Lengyel, 1991). In *nmo*, the male genitalia are normal; that rotation may involve a different mechanism. Several mutations that affect the polarity of bristles, hairs, or both, on cuticular tissues such as leg and wing, also show abnormal eye phenotypes (Gubb and Garcia-Bellido, 1982; Adler et al., 1987). For example, the orientation of photoreceptor clusters in the *disheveled* mutant is often reversed in both the dorsoventral and anterior–posterior axes (Theisen et al., 1994), suggesting that similar mechanisms may be shared by cuticular and eye tissue. However, we found no obvious polarity abnormalities in the cuticular bristles or hairs in *nmo*.

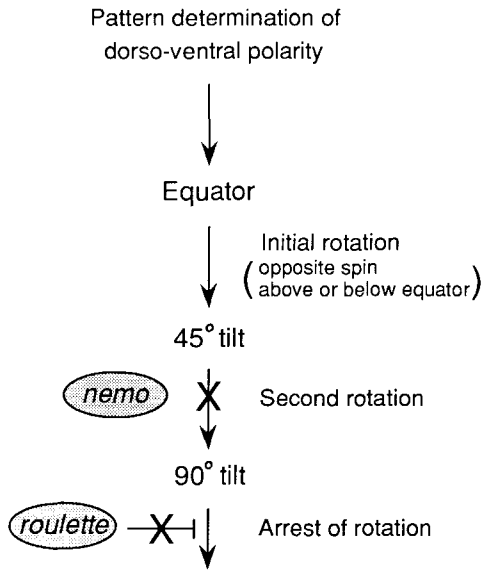

Figure 9. A Two-Step Model for Rotation

Early photoreceptor clusters are initiated to rotate in either a clockwise or a counterclockwise direction, depending on whether they are in the dorsal or ventral half of the eye disc. This initial rotation proceeds to approximately 45°. *nmo*$^+$ is required for further rotation to 90°. Excessive rotation is prevented by the normal function of the *rlt* gene.

Receptor tyrosine protein kinases, such as Drosophila Breathless (Klämbt et al., 1992), c-Kit (Fleischman, 1993), and Met kinases (Stoker et al., 1987; Weidner et al., 1993), are important in signal transduction mechanisms for cell movement, growth, and differentiation. Since signaling of receptor tyrosine kinases is generally mediated by sequential activation of a cascade of serine/threonine protein kinases (Boulton et al., 1991), it is conceivable that the Nmo kinase is in such a pathway. Signal transduction at focal adhesion sites involving tyrosine and serine/threonine protein kinases is important for regulation of cell–substrate adhesion and, ultimately, cell shape and motility (Zachary and Rozengurt, 1992). Nmo protein kinase may thus involve phosphorylation of cytoskeletal elements at such sites.

From the mosaic analysis, *nmo*$^+$ function in any of the photoreceptor cells appears to be sufficient for rotation of an entire 8-cell cluster. This may be because the cells are tightly jointed by cell–cell contacts. Another possibility is that any *nmo*$^+$ photoreceptor cell may send out a short-range signal to activate the others within the cluster. The occasional normal rotation seen in some *nmo*$^-$ photoreceptor clusters at mosaic boundaries may be explained if such a short range signal can also leak to immediately adjacent ommatidia. Indeed, recent evidence suggests that serine/threonine protein kinases are required for expression of diffusible factors, their secretion, or both (Ingham, 1993; Owaki et al., 1993).

Analysis of the *rlt* mutant supports the idea that *nmo*

plays a regulatory role. A remarkable feature of *rlt* is the very broad range of rotation angles, often greater than 90° (Figure 5). Since the 90° rotation in the normal eye is remarkably precise, it is as if the defect in *rlt* is a failure to stop at 90°. The *nmo* mutation largely suppresses that phenotype, suggesting that both genes are involved in a common pathway; *nmo* is epistatic to *rlt*. Our results are consistent with the model in Figure 9. According to this scheme, first, dorsoventral polarity must be established. Rotation is initiated by a signaling mechanism early in photoreceptor cluster formation, the clusters beginning to rotate either clockwise or counterclockwise according to their polarity. Rotation occurs in two steps; the first is *nmo*-independent, while nmo^+ is required for initiation of the second step. Once the rotation has reached 90°, the process must be arrested by the action of rlt^+; without that, rotation may continue unchecked. The model is consistent with the epistatic relation between *nmo* and *rlt*. Nmo kinase is the first molecule that has been identified in this rotation process; other participant molecules are yet to be found. Identification of genes that interact with *nmo* may serve to dissect the mechanisms of cell movement during eye morphogenesis, providing a model system for similar events in other organisms.

Experimental Procedures

Fly Strains and Isolation of *nmo*

nmo^{P1} was a slightly rough eye mutant from an enhancer trap screen of autosomal insertions of a P element containing a *transposase–lacZ* fusion gene P[*lacZ, w*$^+$], as by Bier et al. (1989). Both males and females of the original *nmo* line were sterile as homozygotes. The sterility proved to be due to a separate third chromosome mutation and was removed by recombination. The deficiency stocks $Df(3L)pbl^{K1}$, $Df(3L)pbl^{NR}$, *Df(3L)8*, and *Df(3L)25* were gifts from Drs. G. Hime and R. Saint.

Correlation of the *nmo* phenotype with the P element insertion was tested by reversion tests. *yw;* nmo^{P1}/TM3 Sb females were crossed to ry^{606} *Sb[ry*$^+$*Δ2–3]/TM6b Hu Dr* males, and *yw;* nmo^{P1}/ry^{606} *Sb[ry*$^+$*Δ2–3]* individual males were crossed to *yw; D/TM3 Sb*. Offspring with white eyes were mated to nmo^{P1}*/TM3 Sb* to test for complementation of the *nmo* phenotype. Among 153 w^- revertant lines tested, 73 (48%) had normal eyes.

rlt was isolated by P element mutagenesis and mapped between *th* (3-43.2) and *sr* (3-62.0) by recombination (W. Leiserson and S. B., unpublished data). nmo^{P1} *rlt cu sr e ca* double mutants were generated from nmo^{P1}*/rlt cu sr e ca* females by recombination between *nmo* and *rlt*. Markers and balancers are described in Lindsley and Zimm (1992).

Generation of Mosaic Eyes

To make w^- mutant clones, a w^- excision allele ($nmo^{j147\text{-}1}$) was used. Eyes of $nmo^{P1}/nmo^{j147\text{-}1}$ flies are phenotypically similar to nmo^{P1}/nmo^{P1}. To provide a w^+ marker, P[w^+]33 with an insertion at 70C was used (Carthew and Rubin, 1990). $nmo^{j147\text{-}1}$*/P[w*$^+$*]33* first instar larvae were X-ray irradiated (1000 rad) and screened for w^- patches, which occurred in approximately 1 of 50 eyes. Ommatidia (473, from 15 mosaic patches) were examined by embedding in Epon and sectioning at 1–3 μm.

Histology and Immunocytochemistry

For scanning electron microscopy, flies were dehydrated in an ethanol series, critical point dried, and coated with gold–palladium 80:20. Expression of LacZ was detected with a mouse anti-β-gal monoclonal antibody (Promega) and goat anti-mouse IgG (H + L)–HRP conjugate (Bio-Rad), as by Hart et al. (1990). MAb 22C10 (1:10 dilution), MAb 24B10 (1:10 dilution), and anti-elav (1:500 dilution) were similarly used.

For cobalt staining of pupal eyes, white prepupae were collected and allowed to develop at 20°C. Pupal retinae were dissected and stained with cobalt sulfide, as by Cagan and Ready (1989).

Molecular Cloning

The position of the P[*lacZ, w*$^+$] insertion was determined by chromosome hybridization (Engels et al., 1986) using the biotin-labeled P element as probe. A single insertion in the *nmo* line was thus confirmed, as well as by Southern hybridization to genomic DNA digested with restriction enzymes. Genomic DNA flanking the insertion was isolated by plasmid rescue (Pirrotta, 1986) and used as a probe to screen a cosmid library provided by J. Tamkun. cDNAs were isolated from λgt11 libraries of adult head cDNA (Itoh et al., 1986). Manipulations of DNA and RNA, including Southern and Northern blots, were done according to the protocols of Sambrook et al. (1989).

In situ hybridization to eye imaginal discs was done according to the protocols of Tautz and Pfeifle (1989). Nonradioactive single-stranded DNA probes were made using digoxigenin-11-dUTP by the polymerase chain reaction.

Acknowledgments

Address correspondence to S. B. We thank Rosalind Young and Lynette Dowling for expert technical assistance, and our colleagues for suggestions on the manuscript. We thank William Leiserson for the *rlt* mutant, Gary Hime and Robert Saint for *pbl* deficiency stocks, John Tamkun for the cosmid library, and Kalpana White for anti-elav antibody. We are indebted to an anonymous reviewer for the suggestion to use the P[w^+]33 strain for mosaic analysis and to Todd Laverty of Gerald Rubin's laboratory for furnishing the strain. This research was supported by a postdoctoral fellowship (to K.-W. C.) from the Drown Foundation and grants (to S. B.) from the National Science Foundation (BCS-8908154), the National Eye Institute of the National Institutes of Health (EY0 9278), and the James G. Boswell Foundation.

Received October 20, 1993; revised May 26, 1994.

References

Abbott, M. K., and Lengyel, J. A. (1991). Embryonic head involution and rotation of male terminalia require the *Drosophila* locus *head involution defective*. Genetics *129*, 783–789.

Adler, P. N., Charlton, J., and Vinson, C. (1987). Allelic variation at the *frizzled* locus of *Drosophila*. Dev. Genet. *8*, 99–119.

Bairoch, A., and Claverie, J.-M. (1988). Sequence patterns in protein kinases. Nature *331*, 22.

Baker, N. E., Moses, K., Nakahara, D., Ellis, M. C., Carthew, R. W., and Rubin, G. M. (1992). Mutations on the second chromosome affecting the *Drosophila* eye. J. Neurogenet. *8*, 85–100.

Baker, N. E., and Rubin, G. M. (1992). *Ellipse* mutations in the *Drosophila* homologue of the EGF receptor affect pattern formation, cell division, and cell death in eye imaginal discs. Dev. Biol. *150*, 381–396.

Banerjee, U., and Zipursky, S. L. (1990). The role of cell–cell interaction in the development of the Drosophila visual system. Neuron *4*, 177–187.

Bier, E., Vässin, H., Shephard, S., Lee, K., McCall, K., Barbel, S., Ackerman, L., Carretto, R., Uemara, T., Grell, E., Jan, L. Y., and Jan, Y.-N. (1989). Searching for pattern and mutation in the *Drosophila* genome with a P-*lacZ* vector. Genes Dev. *3*, 1273–1287.

Biggs, W. H., III, and Zipursky, S. L. (1992). Primary structure, expression, and signal-dependent tyrosine phosphorylation of a *Drosophila* homolog of extracellular signal-regulated kinase. Proc. Natl. Acad. Sci. USA *89*, 6295–6299.

Boulton, T. G., Nye, S. H., Robbins, D. J., Ip, N. Y., Radziejewska, E., Morgenbesser, S. D., DePinho, R. A., Panayotatos, N., Cobb, M. H., and Yancopoulos, G. D. (1991). ERKs: a family of protein-serine/threonine kinases that are activated and tyrosine phosphorylated in response to insulin and NGF. Cell *65*, 663–675.

Cagan, R. L., and Ready, D. (1989). The emergence of order in the *Drosophila* pupal retina. Dev. Biol. *136*, 346–362.

Carthew, R. W., and Rubin, G. M. (1990). *seven in absentia*, a gene required for specification of R7 cell fate in the Drosophila eye. Cell *63*, 561–577.

Deuchar, E. M. (1971). The mechanism of axial rotation in the rat embryo: an experimental study in vitro. J. Embryol. Exp. Morphol. *25*, 189–201.

Dietrich, W. (1909). Die Facettenaugen der Dipteren. Z. Wiss. Zool. *92*, 465–539.

Duerr, B., Gawienowski, M., Ropp, T., and Jacobs, T. (1993). MsERK1: a mitogen-activated protein kinase from a flowering plant. Plant Cell *5*, 87–96.

Engels, W. R., Preston, C. R., Thompson, P., and Eggleston, W. B. (1986). *In situ* hybridization to *Drosophila* salivary chromosomes with biotinylated DNA probes and alkaline phosphatase. Bethesda Res. Lab. Focus *8*, 6–8.

Fleischman, R. A. (1993). From white spots to stem-cells: the role of the Kit receptor in mammalian development. Trends Genet. *9*, 285–290.

Fristrom, D. (1976). The mechanisms of evagination of imaginal discs of *Drosophila melanogaster*. III. Evidence for cell rearrangement. Dev. Biol. *54*, 163–171.

Gartner, A., Nasmyth, K., and Ammerer, G. (1992). Signal transduction in *Saccharomyces cerevisiae* requires tyrosine and threonine phosphorylation of FUS3 and KSS1. Genes Dev. *6*, 1280–1292.

Gleichauf, R. (1936). Anatomie und Variabilität des Geschlechtsapparates von *Drosophila melanogaster* (Meigen). Z. Wiss. Zool. *148*, 1–66.

Greenwald, I., and Rubin, G. M. (1992). Making a difference: the role of cell–cell interactions in establishing separate identities for equivalent cells. Cell *68*, 271–281.

Gubb, D., and Garcia-Bellido, A. (1982). A genetic analysis of the determination of cuticular polarity during development of *Drosophila melanogaster*. J. Embryol. Exp. Morphol. *68*, 37–57.

Gumbiner, B. M. (1992). Epithelial morphogenesis. Cell *69*, 385–387.

Hamilton, L. (1969). The formation of somites in *Xenopus*. J. Embryol. Exp. Morphol. *22*, 253–264.

Hanks, S. K., Quinn, A. M., and Hunter, T. (1988). The protein kinase family: conserved features and deduced phylogeny of the catalytic domains. Science *241*, 42–52.

Hart, A. C., Kramer, H., Van Vactor, D. L., Jr., Paidhungat, M., and Zipursky, S. L. (1990). Induction of cell fate in the *Drosophila* retina: the *bride of sevenless* protein is predicted to contain a large extracellular domain and seven transmembrane segments. Genes Dev. *4*, 1835–1847.

Hime, G., and Saint, R. (1992). Zygotic expression of the *pebble* locus is required for cytokinesis during the postblastoderm mitoses of *Drosophila*. Development *114*, 165–171.

Ingham, P. W. (1993). Localized *hedgehog* activity controls spatial limits of *wingless* transcription in the *Drosophila* embryo. Nature *366*, 560–562.

Itoh, N., Slemmon, J. R., Hawke, D. H., Williamson, R., Morita, E., Itakura, K., Roberts, E., Shively, J. E., Crawford, G. D., and Salvaterra, P. M. (1986). Cloning of *Drosophila* choline acetyltransferase cDNA. Proc. Natl. Acad. Sci. USA *83*, 4081–4085.

Klämbt, C., Glazer, L., and Shilo, B.-Z. (1992). *breathless*, a *Drosophila* FGF receptor homolog, is essential for migration of tracheal and specific midline glial cells. Genes Dev. *6*, 1668–1678.

Knighton, D. R., Zheng, J., Ten Eyck, L. F., Ashford, V. A., Xuong, N.-H., Taylor, S. S., and Sowadski, J. M. (1991). Crystal structure of the catalytic subunit of cyclic adenosine monophosphate–dependent protein kinase. Science *253*, 407–414.

Lindsley, D. L., and Zimm, G. G. (1992). The Genome of *Drosophila melanogaster* (San Diego: Academic Press).

Lorincz, A. T., and Reed, S. I. (1984). Primary structure homology between the product of yeast cell division control gene *CDC28* and vertebrate oncogenes. Nature *307*, 183–185.

Melamed, J., and Trujillo-Cenóz, O. (1975). The fine structure of the eye imaginal disc in muscoid flies. J. Ultrastruct. Res. *51*, 79–93.

O'Connell, P., and Rosbash, M. (1984). Sequence, structure, and codon preference of the *Drosophila* ribosomal protein 49 gene. Nucl. Acids Res. *12*, 5495–5513.

Owaki, H., Varma, R., Gillis, B., Bruder, J. T., Rapp, U. R., Davis, L. S., and Geppert, T. D. (1993). RAF-1 is required for T-cell IL2 production. EMBO J. *12*, 4367–4373.

Payne, D. M., Rossomando, A. J., Martino, P., Erickson, A. K., Her, J.-H., Shabanowitz, J., Hunt, D. F., Weber, M. J., and Sturgill, T. W. (1991). Identification of the regulatory phosphorylation sites in pp42/mitogen-activated protein kinase (MAP kinase). EMBO J. *10*, 885–892.

Pearson, W. R., and Lipman, D. J. (1988). Improved tools for biological sequence comparison. Proc. Natl. Acad. Sci. USA *85*, 2444–2448.

Pirrotta, V. (1986). Cloning *Drosophila* genes. In *Drosophila*: A Practical Approach, D. B. Roberts, ed. (Oxford: IRL Press), pp. 83–110.

Ready, D. F. (1989). A multifaceted approach to neural development. Trends Neurosci. *12*, 102–110.

Ready, D. F., Hanson, T. E., and Benzer, S. (1976). Development of the *Drosophila* retina, a neurocrystalline lattice. Dev. Biol. *53*, 217–240.

Reinke, R., Krantz, D. E., Yen, D., and Zipursky, S. L. (1988). Chaoptin, a cell-surface glycoprotein required for Drosophila photoreceptor cell morphogenesis, contains a repeat motif found in yeast and human. Cell *52*, 291–301.

Robinow, S., and White, K. (1991). Characterization and spatial distribution of ELAV protein during *Drosophila melanogaster* development. J. Neurobiol. *22*, 443–461.

Rutishauser, U., and Jessell, T. M. (1988). Cell-adhesion molecules in vertebrate neural development. Physiol. Rev. *68*, 819–857.

Sambrook, J., Fritsch, E. F., and Maniatis, T. (1989). Molecular Cloning : A Laboratory Manual, Second Edition (Cold Spring Harbor, New York: Cold Spring Harbor Laboratory Press).

Stoker, M., Gherardi, E., Perryman, M., and Gray, J. (1987). Scatter factor is a fibroblast-derived modulator of epithelial cell motility. Nature *327*, 239–242.

Tautz, D., and Pfeifle, C. (1989). A non-radioactive in situ hybridization method for the localization of specific RNAs in *Drosophila* embryos reveals translational control of the segmentation gene *hunchback*. Chromosoma *98*, 81–85.

Theisen, H., Purcell, J., Bennett, M., Kansagara, D., Zuhuriidin, A., and Marsh, J. L. (1994). *dishevelled* is required during *wingless* signaling to establish both cell polarity and cell identity. Development *120*, 347–360.

Tomlinson, A. (1985). The cellular dynamics of pattern formation in the eye of *Drosophila*. J. Embryol. Exp. Morph. *89*, 313–331.

Tomlinson, A., and Ready, D. F. (1987). Neuronal differentiation in the *Drosophila* ommatidium. Dev. Biol. *120*, 366–376.

Weidner, K. M., Sachs, M., and Birchmeier, W. (1993). The *Met* receptor tyrosine kinase transduces motility, proliferation, and morphogenic signals of scatter factor/hepatocyte growth factor in epithelial cells. J. Cell Biol. *121*, 145–154.

White, K., and Kankel, D. R. (1978). Patterns of cell division and cell movement in the formation of the imaginal nervous system in *Drosophila melanogaster*. Dev. Biol. *65*, 296–321.

Zachary, I., and Rozengurt, E. (1992). Focal adhesion kinase (p125FAK): a point of convergence in the action of neuropeptides, integrins, and oncogenes. Cell *71*, 891–894.

Zipursky, S. L., Venkatesh, T. R., Teplow, D. B., and Benzer, S. (1984). Neuronal development in the Drosophila retina: monoclonal antibodies as molecular probes. Cell *36*, 15–26.